



HAL
open science

Dual-Cation Electrolytes for High-Power and High-Energy LTO//AC Hybrid Capacitors

Yu Chikaoka, Etsuro Iwama, Tsukasa Ueda, Natsuki Miyashita, Shinichi Seto, Masato Sakurai, Wako Naoi, McMahon Thomas Homer Reid, Patrice Simon, Katsuhiko Naoi

► **To cite this version:**

Yu Chikaoka, Etsuro Iwama, Tsukasa Ueda, Natsuki Miyashita, Shinichi Seto, et al.. Dual-Cation Electrolytes for High-Power and High-Energy LTO//AC Hybrid Capacitors. *Journal of Physical Chemistry C*, 2020, 124 (23), pp.12230-12238. 10.1021/acs.jpcc.0c01916 . hal-03052719

HAL Id: hal-03052719

<https://hal.science/hal-03052719>

Submitted on 10 Dec 2020

HAL is a multi-disciplinary open access archive for the deposit and dissemination of scientific research documents, whether they are published or not. The documents may come from teaching and research institutions in France or abroad, or from public or private research centers.

L'archive ouverte pluridisciplinaire **HAL**, est destinée au dépôt et à la diffusion de documents scientifiques de niveau recherche, publiés ou non, émanant des établissements d'enseignement et de recherche français ou étrangers, des laboratoires publics ou privés.



Open Archive Toulouse Archive Ouverte

OATAO is an open access repository that collects the work of Toulouse researchers and makes it freely available over the web where possible

This is a publisher's version published in: <https://oatao.univ-toulouse.fr/27022>

Official URL:

<https://doi.org/10.1021/acs.jpcc.0c01916>

To cite this version:

Chikaoka, Yu and Iwama, Etsuro and Ueda, Tsukasa and Miyashita, Natsuki and Seto, Shinichi and Sakurai, Masato and Naoi, Wako and Reid, McMahon Thomas Homer and Simon, Patrice  and Naoi, Katsuhiko *Dual-Cation Electrolytes for High-Power and High-Energy LTO//AC Hybrid Capacitors*. (2020) *Journal of Physical Chemistry C*, 124 (23). 12230-12238. ISSN 1932-7447 .

Any correspondence concerning this service should be sent to the repository administrator: tech-oatao@listes-diff.inp-toulouse.fr

Dual-Cation Electrolytes for High-Power and High-Energy LTO//AC Hybrid Capacitors

Yu Chikaoka, Etsuro Iwama,* Tsukasa Ueda, Natsuki Miyashita, Shinichi Seto, Masato Sakurai, Wako Naoi, McMahon Thomas Homer Reid, Patrice Simon, and Katsuhiko Naoi*

 Cite This: *J. Phys. Chem. C* 2020, 124, 12230–12238

 Read Online

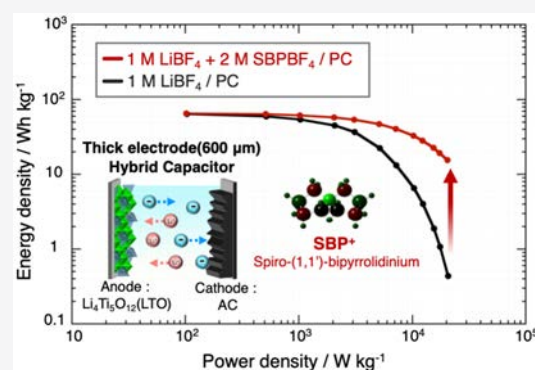
ACCESS |

 Metrics & More

 Article Recommendations

 Supporting Information

ABSTRACT: Dual-cation electrolyte systems, which contain two cations [Li^+ and spiro-1,1'-bipyrrrolidinium (SBP^+), are proposed to enhance the power capability of hybrid capacitors composed of thick $\text{Li}_4\text{Ti}_5\text{O}_{12}$ (LTO) negative ($200\ \mu\text{m}$) and activated carbon (AC) positive electrodes ($400\ \mu\text{m}$), which thus reduces the resistive overvoltage in the system. Detailed studies of the mass transport properties based on the combination of spectroscopy and electrochemical analysis have shown that the presence of SBP^+ , despite slower Li^+ transport in the electrolyte bulk, further reduces overvoltage associated with migration limitation in the thick LTO electrode macropores. This study on the dual-cation electrolyte quantifies the influence of the addition of a supporting electrolyte and shows interest in SBPBF_4 addition for increasing the output power density of hybrid capacitors with a thick electrode configuration.



1. INTRODUCTION

Electric double layer capacitors (EDLCs), also known as supercapacitors, are energy-storage devices (ESDs) boasting speeds and lifespans far greater than those of batteries, but whose practical applications are limited by their moderate energy densities. This has motivated intense efforts to improve the storage capacity of EDLCs.^{1,2} Although conventional EDLCs are symmetric devices that consist of two identical activated-carbon (AC) electrodes, much recent research has focused on asymmetric/hybrid supercapacitors that pair an AC positive electrode with a high-capacity faradaic negative electrode made from a lithium intercalation compound such as $\text{Li}_4\text{Ti}_5\text{O}_{12}$ (LTO).^{3,4} The adoption of hybrid structures succeeds in increasing the energy density.^{5,6} Besides designing another EES device system such as dual-ion batteries, which apply anion-intercalation into carbon positive electrodes,^{7,8} further enhancement can be expected by simply increasing electrode thickness from a few tens to hundreds of micrometers. However, the use of such thick electrodes is detrimental to the power capability with an increase in ionic resistance of the electrodes.^{9,10} Furthermore, the limited choice of electrolytic salts available for hybrid capacitors made the situation ever more complex. Ideally, one would like to use LiPF_6 , the electrolyte most commonly used in Li-ion batteries (LIBs), but this is incompatible with the choice of AC as an electrode material, as LiPF_6 is unstable against the moisture coming from AC. Instead, supercapacitors with AC electrodes must use alternative electrolytes, such as LiBF_4 ,^{3,4,11} whose ionic conductivity is less than LiPF_6 , and the search for high-

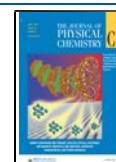
conductivity supercapacitor electrolytes is the focus of intense research efforts.

One of the developed approaches to improve the rate capability of LIBs is to enhance the Li^+ transport (diffusion, migration) by using alternative lithium electrolytic salts or solvents.¹² Among them, the superconcentrated lithium-salt electrolyte, generally dissolving over 4–5 M of electrolytic salts, is a topic that has been intensively researched recently to improve power performances as well as the potential window of electrolytes.^{13,14} Such superconcentrated electrolytes are reported to suppress the concentration polarization thanks to the improvement of Li^+ transport.^{13,14} Using thick electrodes, however, their low ionic conductivity may be detrimental to the power performances, while several issues are expected for their practical applications, such as difficulty in the electrolyte injection process due to their very high viscosity.¹⁵ In this Article, we develop an alternative route through the addition of a supporting electrolyte to increase the ionic transport properties, mainly aimed at ESDs using thick electrodes. LTO//AC hybrid capacitors with a total electrode thickness of $600\ \mu\text{m}$ were assembled and tested in electrolyte containing various amounts of a supporting electrolyte, and the rate

Received: March 6, 2020

Revised: May 11, 2020

Published: May 19, 2020



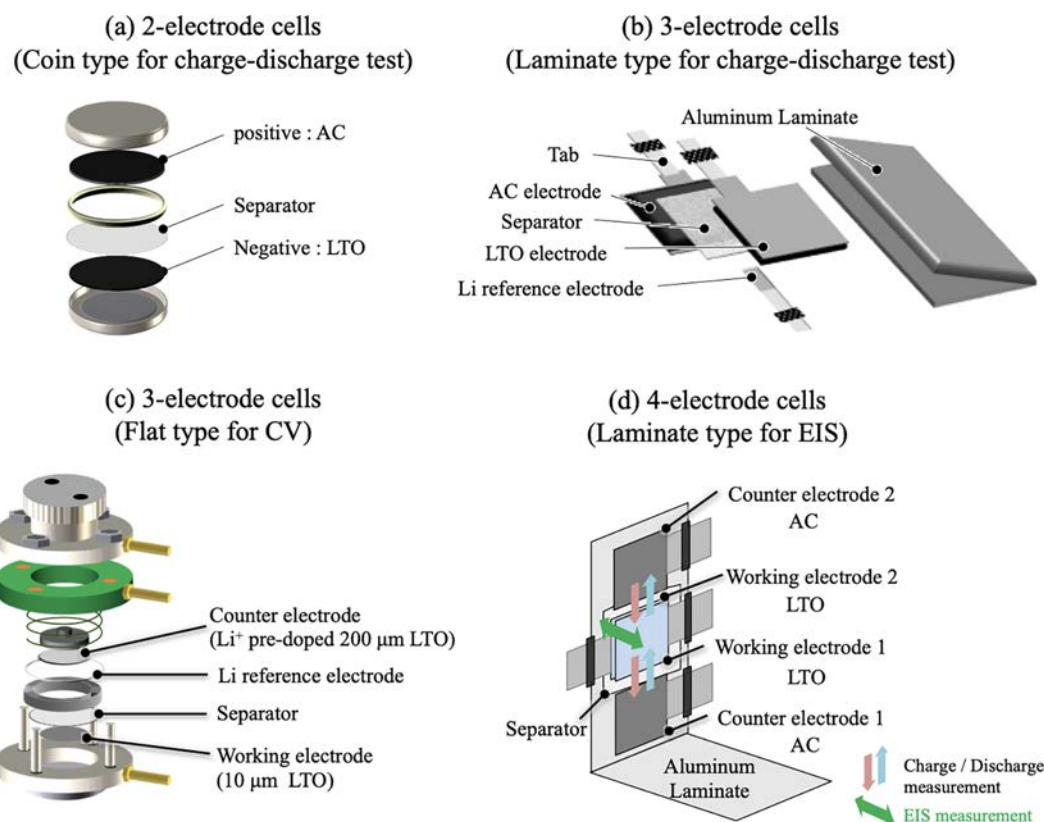


Figure 1. Schematic illustrations of cell configurations prepared in this work: (a) two-electrode cells (coin type for charge–discharge test), (b) three-electrode cells (laminate type for charge–discharge test), (c) three-electrode cells (flat type for CV), and (d) four-electrode cells (laminate type for EIS).

performance was investigated in detail. Spiro-1,1'-bipyrrrolidinium tetrafluoroborate (SBPBF₄) was selected as a supporting electrolytic salt thanks to its high ionic dissociation to be added into LiBF₄-based electrolytes. We evidenced that the presence of a supporting SBPBF₄ electrolyte significantly improved the electrochemical performance of hybrid capacitors using a few-100 μm-thick LTO electrodes despite the decrease in Li⁺ transport number. We expect that our finding may offer flexible choices in electrolyte composition, especially in case of using thick electrodes attaining both high power and energy density of ESDs.

2. EXPERIMENTS

2.1. Electrolyte Preparation. Electrolytes (water content < 20 ppm) were prepared by dissolving 1 M lithium tetrafluoroborate (battery grade LiBF₄, Kishida Chemicals, Japan) and *x* M spiro-1,1'-bipyrrrolidinium tetrafluoroborate (SBPBF₄, Japan Carlit, 0 < *x* < 3) in propylene carbonate (PC, battery grade, Kishida Chemicals, Japan). Prior to use, prepared electrolytes were stirred under an Ar-filled glove box (UNICO) overnight.

2.2. Physicochemical Properties of Electrolytes. Ionic conductivity of the electrolytes was measured using a conductivity meter setup (Mettler Toledo, S230) with a four-electrode Pt conductivity sensor (Mettler Toledo, InLab 710) at *T* = 25 °C. The viscosity of the electrolytes was measured using a digital viscometer (Brookfield, DV-II+pro). All of the viscosity measurements were conducted at *T* = 25 °C. The volume of electrolytes was set to be 1 mL, and the dynamic viscosity was calculated from the obtained shear stress

at the shear rate where the spindle experienced 10% of the maximum torque of the equipment.

2.3. Self-Diffusion Coefficients of Electrolytes. Self-diffusion coefficients of electrolytes were measured by pulsed-gradient spin-echo nuclear magnetic resonance (PGSE-NMR), with a 400 MHz NMR spectrometer (JEOL, JNM-ECZR) equipped with JEOL gradient probes at room temperature (*T* = 25 °C). Self-diffusion coefficients *D* were calculated according to eq 1.¹⁶

$$\ln(S/S_0) = -\gamma^2 g^2 \delta^2 D (\Delta - \delta/3) \quad (1)$$

Here, S/S_0 [–] is the echo attenuation, γ [s⁻¹ T⁻¹] is the gyromagnetic field, g [T m⁻¹] is the strength, δ [s] is the duration of the gradient pulse, and Δ [s] is the interval between the gradient pulse. Each NMR microtube (ϕ = 5 mm, Shigemi) was filled with prepared electrolytes (about 5 mm height, 70 μL) and sealed in the dry room before any measurements. PGSE-NMR measurements were performed by applying a magnetic field gradient pulse from 1.0 to 13.5 T m⁻¹ with a 50 ms interval between each gradient pulse. Self-diffusion coefficients of Li⁺ (⁷Li), SBP⁺ (¹H), and BF₄⁻ (¹⁹F) in electrolytes were calculated from the obtained slopes of the intensity against the magnetic field gradient strength.

2.4. Electrode Preparation. Li₄Ti₅O₁₂ (LTO, Toho Titanium) and activated carbon (AC, YP-50F, Kuraray) were used as positive and negative active material electrodes, respectively. Previous experiments by our group¹⁷ have shown that an LTO//AC mass ratio of 0.79 (=exhibited capacity ratio of 3.5) resulted in optimized performance of the cell, corresponding to electrode loading mass/thickness of 13.3

Table 1. Measured Values of Ionic Conductivity, Viscosity, and Self-Diffusion Coefficient for Single- and Dual-Cation Electrolytes of Various Additive Concentrations^a

	ionic conductivity/mS cm ⁻¹	viscosity/cP	self-diffusion coefficient/ 10 ⁻¹⁰ m ² s ⁻¹			transport number/–			individual ionic conductivity/mS cm ⁻¹		
			Li ⁺	SBP ⁺	BF ₄ ⁻	Li ⁺	SBP ⁺	BF ₄ ⁻	Li ⁺	SBP ⁺	BF ₄ ⁻
1 M LiBF ₄ /PC	3.57	6.77	0.88	1.26	0.41	0.59	1.47	2.10			
1 M LiBF ₄ + 1 M SBPBF ₄ /PC	5.89	11.35	0.56	1.03	0.92	0.16	0.30	0.54	0.96	1.77	3.15
1 M LiBF ₄ + 2 M SBPBF ₄ /PC	7.79	18.41	0.30	0.62	0.52	0.10	0.40	0.50	0.76	3.12	3.91
1 M LiBF ₄ + 3 M SBPBF ₄ /PC	7.36	30.65	0.16	0.35	0.30	0.07	0.43	0.50	0.49	3.19	3.68

^aIn this table, “ionic conductivity” refers to the measured ionic conductivity of the electrolytic solution, while “individual ionic conductivity” refers to the ionic conductivity times the transport number.

mg cm⁻²/200 μm (LTO) and 16.8 mg cm⁻²/400 μm (AC). The total electrode thickness of LTO and AC electrodes ($\phi = 16$ mm) was set to be 600 μm, with the aim to maximize the energy density for 2032 coin-type cells. Each active material was mixed with 10 wt % of Ketjen Black conducting additive (KB, ECD-600JD, Ketjen Black International) and 10 wt % of polytetrafluoroethylene binder (PTFE, Du Pont-Mitsui Fluorochemicals Co.), and then roll-pressed to make electrodes with fixed thickness and density (400 ± 10 μm and 0.41 g cm⁻³ for AC, 200 ± 10 μm and 0.68 g cm⁻³ for LTO). LTO and AC electrodes were dried at 200 °C under vacuum (<−0.1 MPa) overnight and were further pasted in dry room on current collectors using Hitasol AB-1 (Hitachi Chemical) as a conductive adhesive to prepare the electrodes. Two different current collectors were selected for different types of cells (see section 2.5): stainless steel (SUS316L, 1 mm thick) for 2032 coin-type and flat-type cells, and etched aluminum foil (40 μm thick) for laminated-type cells. Prepared electrodes were then dried at 200 °C under vacuum (<−0.1 MPa) overnight before cell assembly. For cyclic voltammetry (CV) analysis, thin LTO electrodes with a loading of 1.23 mg cm⁻² were prepared by coating LTO slurry on an etched aluminum foil (20 μm thick). 80 wt % of LTO powders, 10 wt % of KB as conductive agent, and 10 wt % of polyvinylidene fluoride (PVDF) binder were all dissolved in 1-methyl-2-pyrrolidone (NMP) to prepare the slurry.

2.5. Cell Assembly and Electrochemical Characterization. For electrochemical characterization, we used four different cell designs shown in Figure 1a–d. 2032 coin-type cells (Figure 1a) were assembled to achieve charge/discharge experiments of LTO//AC hybrid capacitor cells. After being dried overnight, electrodes and cellulose separator (35 μm thickness with 75% of porosity,¹⁸ Nippon Kodoshi (NKK)) were soaked in electrolytes and then put under a vacuum (−70 kPa) for 10 min to ensure electrolyte impregnation. The wet separator then was sandwiched by LTO and AC electrodes, placed into stainless cell cases, and sealed to obtain hybrid capacitor coin cells. Constant current (CC) charge–discharge cycles were achieved within the voltage range of 0–3.0 V by potentiostat units (HJ 1001 SD 8, Hokuto). All of the cells were placed in a climatic chamber to keep $T = 25$ °C. The discharge current densities ranged from 1 to 100 mA cm⁻², while the applied charge current was kept constant at 1 mA cm⁻². Prior to any tests, cells were pre-cycled two times at a slow current density of 0.1 mA cm⁻² within a 0–3.0 V voltage window.

The three-electrode laminate-type cells (5 cm × 11 cm, Figure 1b) were assembled by following the same procedure as was used for the 2032 coin-type cells, with the addition of a lithium metal reference electrode, to track the potential of

negative LTO and positive AC electrodes separately during LTO//AC hybrid cells' operation. A small piece of lithium metal was added as a reference electrode, and LTO and AC electrodes (2 cm × 4 cm) were pasted on an etched aluminum foil (40 μm thick). Assembled cells were charged and discharged at the same conditions as those applied for the coin-type cells.

For CV analysis on LTO electrode, we assembled three-electrode flat-type cells (Figure 1c) using 10 μm-thick LTO working, 200 μm-thick LTO counter, and lithium metal electrodes. Here, we chose the overcapacitive 200 μm-thick LTO electrode as the counter, which was Li predoped in use, to exclude any influence of AC positive electrode. CV measurements (VersaSTAT 3, AMETEK) were conducted at different scan rates from 0.278 to 278 mV s⁻¹, so that scan times changed from 7200 s (corresponding to 0.5C) to 7.2 s (500C).

EIS measurements were performed on LTO//LTO symmetric laminate-type cells (Figure 1d), to evaluate the ionic and charge-transfer resistance of the LTO electrodes. The details for the cell preparation are described in Figure S1. In the LTO//LTO symmetric cells, two LTO electrodes (200 μm thick and 4 cm² each, working electrodes 1 and 2) were placed in the center and sandwiched between a cellulose separator, while two AC electrodes (400 μm thick and 4 cm² each, counter electrodes 1 and 2) were respectively placed in the upper and lower parts of the LTO electrodes. Such a cell configuration allows us to switch two different measurement modes by just changing the connection of the cable: (i) charge and discharge mode [state of charge (SOC) control of LTO] in LTO//AC hybrid capacitor configuration with series-connected two LTO and two AC, respectively, and (ii) EIS measurement mode in LTO//LTO symmetric configuration using only two LTO electrodes with the same SOC condition. The merit of our cell configuration is that there is no need to disassemble the cells prior to EIS measurements unlike in previously reported symmetric cell configurations. For the measurements, first, cells were pre-cycled in LTO//AC hybrid capacitor mode for 2 cycles between 0 and 3.0 V at constant-current (CC) charge (0.1 mA cm⁻²) and CC discharge (0.1 mA cm⁻²) mode. The cells then were charged to 2.7 V at constant-current and constant-voltage (CC–CV) mode with a current density of 0.1 mA cm⁻², and the potential was held during 12 h at 2.7 V. EIS measurements using LTO//LTO symmetric cells were carried out at OCV (fully discharged state) and 1.55 V vs Li/Li⁺ at five different temperatures (25, 30, 35, 40, and 45 °C), using a perturbation signal of ±10 mV within a frequency range from 0.01 Hz to 65.5 kHz. The generalized finite length Warburg element short-circuit

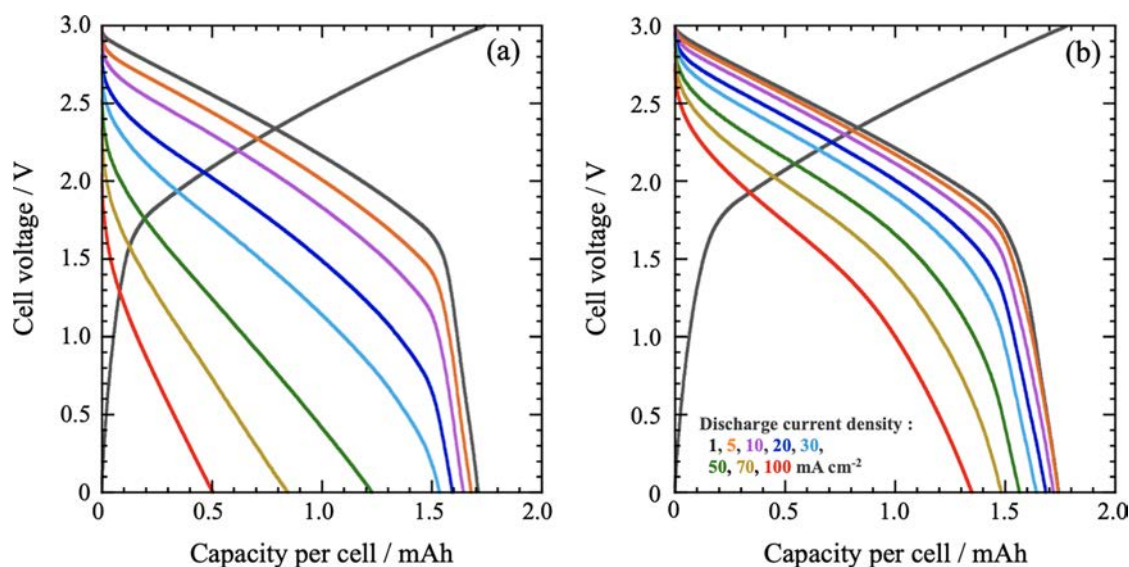


Figure 2. Results of performance tests for two-electrode cells: (a) single-cation (1 M LiBF₄/PC) or (b) dual-cation (1 M LiBF₄ + 2 M SBPBF₄/PC) electrolytes at discharge current densities ranging from 1 to 100 mA cm⁻².

terminus (W_s) was used for fitting of impedance spectra at the SOC of 25%.⁸

3. RESULTS AND DISCUSSION

3.1. Physical Properties of Single- and Dual-Cation Electrolytes. Table 1 lists the ionic conductivity and viscosity of LiBF₄ (single-cation) electrolytes with various concentrations of SBPBF₄ (dual-cation electrolytes), as well as self-diffusion coefficients, transport numbers, and ionic conductivities of ions. The whole ionic conductivity increases significantly as the SBPBF₄ concentration increases to 2 M and then further reaches a plateau. The viscosity of the dual-cation electrolytic solutions is 2–4 times greater than that in the single-cation electrolyte. The diffusion coefficients of all ionic species (Li⁺, BF₄⁻, and SBP⁺) decrease with increasing SBPBF₄ concentration. Also, the diffusion coefficient of SBP⁺ exceeds that of Li⁺ at all SBPBF₄ concentrations; this is assumed to originate from the smaller ionic radius of SBP⁺ as compared to that of solvated Li⁺.

Transport numbers t_x for ion species ($x = \text{Li}^+$, SBP⁺, and BF₄⁻) were calculated from eq 2:¹⁶

$$t_x = N_x D_x / (N[\text{Li}^+]D[\text{Li}^+] + N[\text{BF}_4^-]D[\text{BF}_4^-] + N[\text{SBP}^+]D[\text{SBP}^+]) \quad (2)$$

Here, N_x and D_x are respectively the number of carrier and the self-diffusion coefficient for ion species x ($x = \text{Li}^+$, SBP⁺, and BF₄⁻). Practically, because the number of each carrier, Li⁺, SBP⁺, and BF₄⁻, cannot be estimated within a dual-cation electrolyte, N_x of each carrier was determined from the original concentration of the prepared electrolytes. As the SBPBF₄ concentration increases, the transport number of Li⁺ decreases, while that of SBP⁺ increases. Ionic conductivities of the three ionic species σ_x ($x = \text{Li}^+$, SBP⁺, and BF₄⁻) were calculated from eq 3:

$$\sigma_x = \sigma_{\text{EIS}} \times t_x \quad (3)$$

As the SBPBF₄ concentration increases, both the transport number and the ionic conductivity of Li⁺ decrease, indicating reduced conductivity of Li⁺ in the bulk electrolytic solution,

while both parameters of SBP⁺ increase and are superior to those of Li⁺. By addition of 2 M SBPBF₄, the contribution of SBP⁺ and BF₄⁻ to the total ionic conductivity reaches 90%.

3.2. Performance Tests for Two-Electrode Cells. Figure 2 shows the experimental charge–discharge curves for the hybrid capacitors assembled with 200 μm-thick LTO negative and 400 μm-thick AC positive electrodes using single-cation (1 M LiBF₄/PC) and dual-cation (1 M LiBF₄ + 2 M SBPBF₄/PC) electrolytes. The discharge curves at 1 mA cm⁻² for both electrolytes exhibit a sloping profile, as a result of the combination of a constant potential discharge (LTO negative electrode) and a capacitive sloping signature (AC positive electrode). At higher discharge currents (>20 mA cm⁻²), the mean discharge voltages for the dual-cation electrolyte are much higher as compared to those for the conventional single-cation electrolyte. Note that the added SBPBF₄ concentration in this study was fixed at 2 M after the dependency of cell power performances on the SBPBF₄ concentration from 0 to 3 M added in 1 M LiBF₄/PC was examined (see Figure S2).

The smaller polarization observed for the dual-cation electrolyte shows evidence of improved transport properties (decreased ohmic drop) and/or improved electrochemical reaction kinetics. Both the IR drop, due to bulk electrolyte resistance, and the polarization in the thick electrode are significantly smaller when the dual-cation electrolyte is used. These results are supported by the change of the rate-capability on the electrode thickness (see Figure S3a–c). As shown in Figure S3a, for thin electrodes (LTO = 40 μm, AC = 80 μm), no difference in rate capability was observed for the electrolytes with or without SBPBF₄. The thicker were the electrodes (Figure S3b,c), the greater was the difference between the two electrolytes: for thicker electrodes (400 μm-thick LTO), 70% of the capacity was maintained at 3.3 mA g⁻¹ in the dual-cation electrolyte, while the capacity was null for the single-cation reference cell. From the above findings, the use of dual-cation electrolytes results in significant improvements in cell performance due to a drastic decrease of the electrode polarization. For example, at a current density of 100 mA cm⁻², the single-cation capacity retention was 30% at 1 mA cm⁻², as compared to 78% for the dual-cation system.

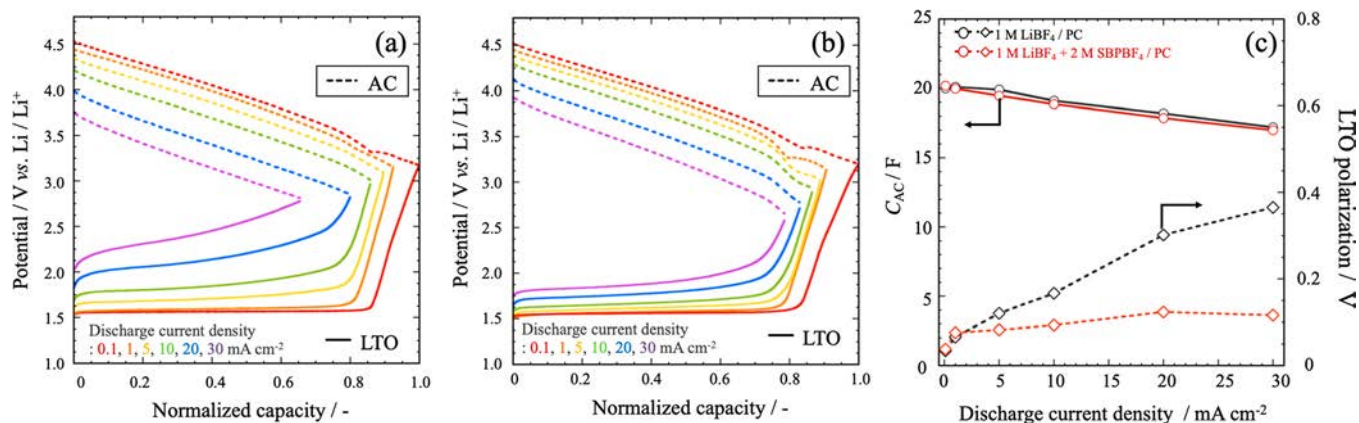


Figure 3. Discharge curves for three-electrode cells with electrolytes of (a) single-cation (1 M LiBF₄/PC) or (b) dual-cation (1 M LiBF₄ + 2 M SBPBF₄/PC) electrolytes at discharge current densities ranging from 0.1 to 30 mA cm⁻². The horizontal axis is normalized to a capacity of 0.1 mA cm⁻² to clarify the comparison of polarization behavior. (c) Static capacitance on the AC positive electrode side, and polarization of the LTO negative electrode side, versus discharge current density. LTO polarization corresponds to the difference in LTO potential at SOC 50% at between 0.1 mA cm⁻² and a given current density. Estimated values were normalized by subtracting IR drops.

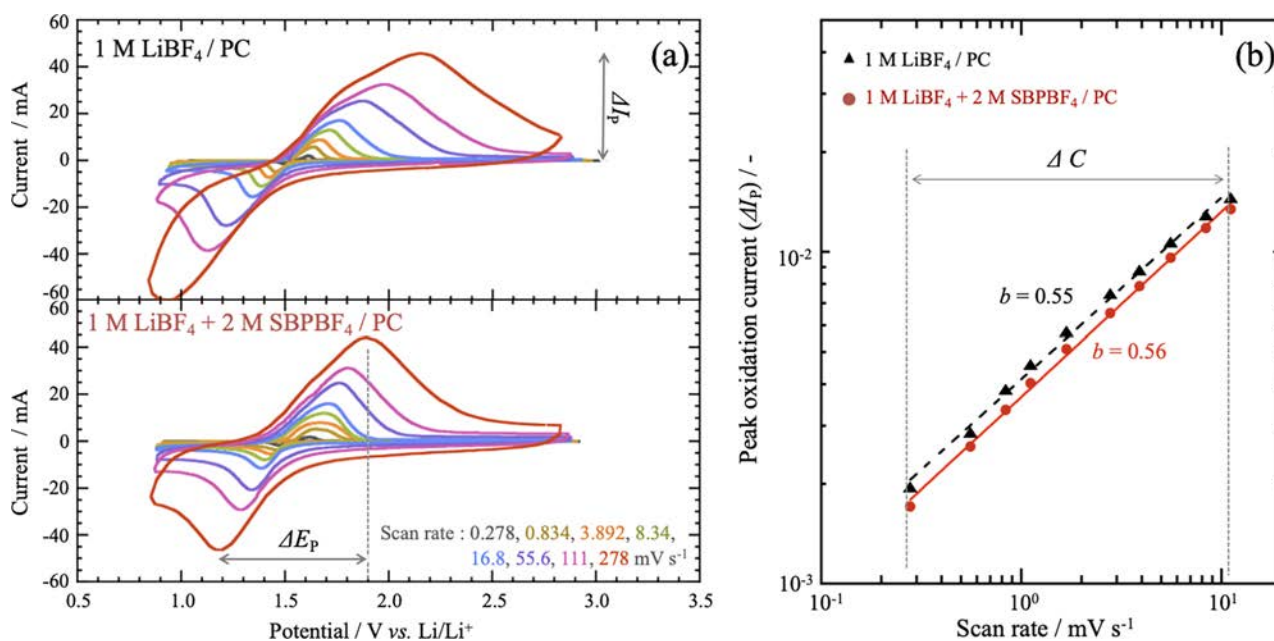


Figure 4. (a) Cyclic voltammograms of LTO for single-cation (1 M LiBF₄/PC) and dual-cation (1 M LiBF₄ + 2 M SBPBF₄/PC) electrolytes at different scan rates from 0.278 to 278 mV s⁻¹ (0.5–500C). (b) Plots of peak oxidation current versus scan rate and obtained *b* factor for the two electrolyte systems. The ΔC corresponds to the region where linearity can be seen for two electrolytes, extracted from the original plots shown in Figure S4.

3.3. Performance Tests for Three-Electrode Cells.

Three-electrode experiments were achieved to study the electrochemical behavior of each electrode separately. Figure 3 compares the experimental discharge curves obtained in single-cation and dual-cation electrolytes. The discharge capacity is normalized to the capacity measured at 0.1 mA cm⁻² discharge current density. First, potential drops observed when switching on the current (IR drops) are reduced in the dual-cation system for both AC positive and LTO negative electrodes. The capacitance of the AC positive electrode was calculated from the slopes of the discharge curves and plotted versus the discharge current (Figure 3c, upper part). As can be seen from the figure, there is no difference in calculated capacitances between the two electrolytes, indicating that the kinetics of ion adsorption/desorption at the surface of the AC

electrode is kept the same. Differently, three-electrode measurements show that the polarization at the LTO negative electrode is greatly decreased in the dual-cation electrolyte at high current density, as can be seen in Figure 3c (lower part). To clearly understand the origin of such a polarization decrease on the LTO electrode, dedicated electrochemical measurements such as CV and EIS were conducted, and the results are shown in the following sections.

3.4. CV Measurements. Figure 4a shows CVs of the LTO negative electrode at different potential scan rates. CV experiments were recorded at potential scan rates from 0.278 to 278 mV s⁻¹, so that scan times changed from 7200 s (0.5C) to 7.2 s (500C). At a slow scan rate (0.278 mV s⁻¹; 0.5C), we observe the typical electrochemical behavior for the LTO electrode in both single- and dual-cation electrolytes, showing

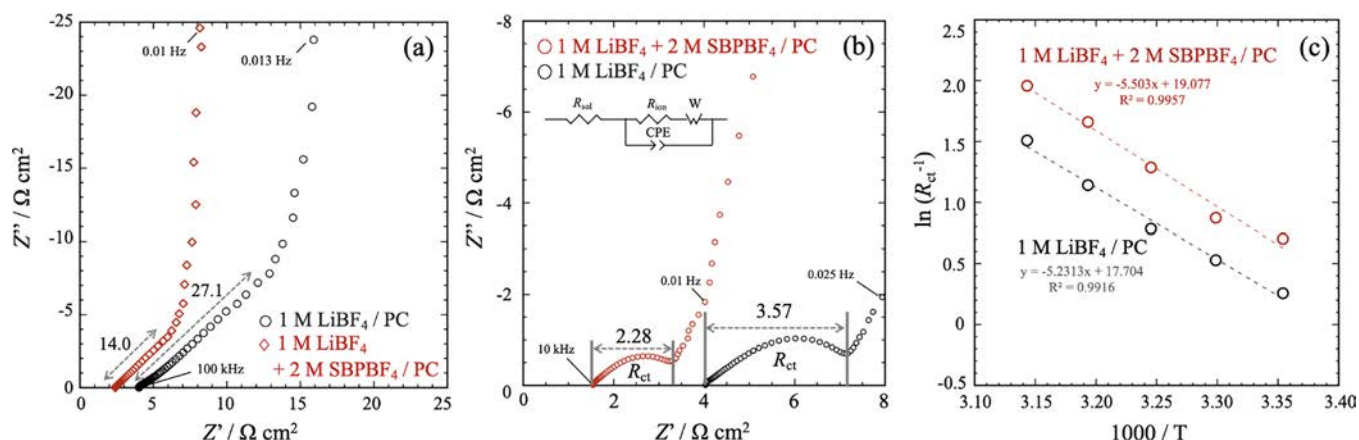


Figure 5. EIS spectra using LTO//LTO symmetric cells for single-cation (1 M LiBF₄/PC) and dual-cation (1 M LiBF₄ + 2 M SBPBF₄/PC) electrolytes (a) when delithiated (SOC of LTO = 0%, 0 V vs Li/Li⁺ in LTO//AC) and (b) when lithiated (SOC = 25%, 2.7 V vs Li/Li⁺ in LTO//AC). (c) Arrhenius plot of the charge-transfer resistance R_{ct} observed in the EIS spectra shown in (b).

similar capacity values of ca. 170 mAh g⁻¹. Differently, at fast scan rates (16.8–278 mV s⁻¹; 30–500C), a distorted electrochemical signature was obtained, together with peak potential shifts for the single-cation system, which was reduced for the dual-cation cell. Figure S4 plots the difference between the peak potentials versus the scan rate. At slow scan rates (0.278–11.1 mV s⁻¹; 0.5–20C), the plots for the single- and dual-cation systems are similar. At high potential scan rates (16.8–278 mV s⁻¹), however, the plot for the single-cation system is much steeper than that for the dual-cation case, thus evidencing a change in the electrochemical behavior.

Figure 4b shows the change of the oxidation peak current of LTO versus the scan rate (up to 11.1 mV s⁻¹), which can be expressed as eqs 4 and 5:

$$I_p = av^b \quad (4)$$

$$\log I_p = \log a + b \log v \quad (5)$$

where v is the scan rate, a is a constant that includes the diffusion coefficient, and b is a dimensionless constant taking values in the range 0.5–1. A b value close to 0.5 shows a diffusion-limited process, that is, a limitation by the diffusion of Li⁺ in the solid LTO, while values close to 1 correspond to a nondiffusion limited, surface-like redox process.¹⁹ For potential scan rates below 16.8 mV s⁻¹, similar b values, close to 0.5, were found for the LTO electrode in both electrolytes, without a significant difference in vertical offset. This means that the solid-state diffusion of Li⁺ does not differ significantly between the two electrolytes, and thus the LTO reaction kinetics are limited by the solid diffusion of Li⁺. In contrast, at higher potential scan rates (>16.8 mV s⁻¹, Figure S4), the behavior of the two systems differs significantly: the growth of the overvoltage magnitude with a scan rate becomes exponential in the single-cation case, but remains only linear in the dual-cation case. The different behaviors of the single- and dual-cation electrolytes may then be attributed to the Li⁺ transport (migration) of the electrolyte in the LTO electrode.

3.5. Impedance Measurements for Symmetric Cells.

Electrochemical impedance spectroscopy (EIS) experiments have been achieved to obtain further detailed insights on the transport versus kinetic limitations. LTO//LTO symmetric cells (Figure 1d) were applied for EIS experiments, to focus on the LTO electrode resistances, which can be divided into two

main contributions: the electrolyte ionic resistance within electrode macropores (R_{ion}) and the Li⁺ charge-transfer resistance at the electrode/electrolyte interface (R_{ct}). Note that assembled LTO//LTO symmetric cells were accustomed to easily switch measurement modes between LTO//AC hybrid capacitor cell cycling (SOC control of LTO) and EIS on LTO//LTO symmetric cells without any disassembling of the cells (see Experiments and Figure S1). Prior to any EIS measurements, all of the cells were precycled (two cycles) in the LTO//AC hybrid capacitor connection mode between 0.0 and 3.0 V. EIS measurements then were conducted using the LTO//LTO symmetric design in both the delithiated (SOC of LTO = 0%, 0 V in LTO//AC) and the lithiated (SOC = 25%, 2.7 V in LTO//AC) states. Figure 5a shows the EIS spectra of LTO//LTO symmetric cells in the delithiated state (SOC = 0%). The R_{ion} measured at high frequency at the intercept of the plot on the real axis²⁰ for the dual-cation electrolyte (R_{ion} : 14.0 $\Omega \text{ cm}^2$) is about 2 times less as compared to the single-cation electrolyte (R_{ion} : 27.1 $\Omega \text{ cm}^2$), which well agrees with the difference in conductivity between two electrolytes. No high frequency loop related to the SEI layer formation on the LTO surface can be observed, and the plot corresponds to a blocking porous electrode behavior in the absence of Li⁺ reaction. Figure 5b shows the EIS spectra conducted on LTO//LTO symmetric cells at the lithiated state (SOC = 25%). A semicircle can be seen in Figure 5b, which corresponds to the R_{ct} .²¹ The value of the R_{ct} was estimated by an equivalent circuit given in the inset of the figure. Overall, the R_{ct} values for the LTO negative electrode for both of the electrolytes were 6–7 times smaller as compared to the R_{ion} values. The obtained results well agree with the previous report¹⁰ that shows that the main contribution to the electrode resistance changes from R_{ct} for thin-film electrodes to R_{ion} for thick-film electrodes. This is further supported by the fact that, using thin-film electrodes (LTO, 40 μm ; AC, 80 μm), the high conductivity of the dual-cation electrolyte does not make a major difference in the discharge characteristic (Figure S3). The R_{ct} then was found to be lower in the dual-cation electrolyte (R_{ct} : 2.28 $\Omega \text{ cm}^2$) than in the single-electrolyte system (R_{ct} : 3.57 $\Omega \text{ cm}^2$), indicating faster electrochemical kinetics. The activation energy E_a of the reaction at the LTO negative electrode was calculated using eq 6:²²

$$\ln(1/R_{\text{ct}}) = -E_a/R \cdot 1/T + \ln A_0 \quad (6)$$

where R is the gas constant, T is the absolute temperature, and A_0 is the pre-exponential factor, which is a temperature-independent constant. The change of $\ln(1/R_{ct})$ versus $1/T$, plotted in semilog scale in Figure S5, shows nearly identical slopes but with constant offset, suggesting nearly equal activation energies E_a but significantly different pre-exponential factors A_0 for the two electrolytes.

Table 2 lists the activation energies E_a and pre-exponential factors A_0 calculated from the Arrhenius plots (eq 6). Indeed,

Table 2. Activation Energies and Pre-exponential Factors for Single-Cation (1 M LiBF₄/PC) and Dual-Cation (1 M LiBF₄ + 2 M SBPBF₄/PC) Electrolytes

	activation energy/ kJ mol ⁻¹	pre-exponential factor/–
1 M LiBF ₄ /PC	49.0	e ^{20.0}
1 M LiBF ₄ + 2 M SBPBF ₄ /PC	51.9	e ^{21.6}

no significant difference in E_a is observed between the two electrolytes; the obtained values are consistent with previous works reporting an activation energy E_a of approximately 50 kJ mol⁻¹ for reactions at LTO negative electrode using 1 M LiPF₆/EC + DMC as the electrolyte.^{23,24} This result indicates that the solvation shells of Li⁺ are more or less the same with and without SBPBF₄, showing that the supporting electrolyte does not change the kinetics of Li⁺ intercalation itself. Raman (Figure S5) and NMR (Figure S6) spectroscopies further support the fact that no drastic change of solvation structure was observed following the addition of SBPBF₄ to the electrolyte. However, the pre-exponential factor A_0 increased with an addition of SBPBF₄ by a factor of 4.95 from e²⁰ to e^{21.6}.

To clarify this, we have considered several hypotheses (ionic charge carriers, number of active sites, SEI layer, and ionic conductivity), and, among them, we concluded that the ionic conductivity is responsible for the increase in pre-exponential factor based on the following discussion.

Ionic Charge Carriers. The ionic charge carriers density, that is, dissociated Li⁺ concentration, affects the pre-exponential factor; the higher is the concentration of Li⁺, the higher is A_0 .²⁵ The apparent degree of dissociation of the various electrolytes, Haven ratio (H_R), was calculated on the basis of the molar ionic conductivity obtained by EIS and NMR (see Supporting Information [Haven ratio]).²⁶ As shown in Table 3, the H_R of the dual-cation electrolyte decreases with the addition of SBPBF₄. Considering the fact that the molar concentration of Li⁺ is fixed at 1.0 M for all electrolyte compositions, the dissociation degree of Li⁺ decreases with increasing SBPBF₄ concentration. So, the

Table 3. Molar Conductivity Evaluated from EIS (λ_{EIS}) and from NMR (λ_{NMR}), and the Haven Ratio for Single-Cation (1 M LiBF₄/PC) and Dual-Cation (1 M LiBF₄ + α M SBPBF₄/PC, $\alpha = 1-3$) Electrolytes of Various Additive Concentrations

	$\lambda_{\text{EIS}}/$ mS cm ⁻¹	$\lambda_{\text{NMR}}/$ mS cm ⁻¹	Haven ratio/–
1 M LiBF ₄ /PC	3.40	8.1	0.42
1 M LiBF ₄ + 1 M SBPBF ₄ /PC	2.95	12.9	0.23
1 M LiBF ₄ + 2 M SBPBF ₄ /PC	2.60	11.6	0.22
1 M LiBF ₄ + 3 M SBPBF ₄ /PC	1.84	9.2	0.20

number of Li⁺ carriers cannot be the origin of the increased pre-exponential factor observed for this system, and we have to determine another reason for why the pre-exponential factor increased.

Number of Active Sites. The number of active sites that can intercalate and deintercalate²⁷ Li⁺ ions has a direct influence on the pre-exponential factor. However, because our experiments use the same LTO electrodes for both the single- and the dual-cation systems, the number of active sites is presumably identical in the two systems.

SEI Layer. The charge-transfer resistance is affected by the formation of SEI films.²⁸ To see whether any SEI films formed in a dual-cation system affected the EIS spectra, we compared EIS spectra on LTO//LTO symmetric cells before and after exchanging electrolytes between single-cation and dual-cation electrolyte systems (Figure S7). The obtained EIS spectra were almost identical for both electrolytes. Thus, the presence of SEI film cannot explain the difference in the pre-exponential factor.

Ionic Conductivity. From above, the increase of the pre-exponential factor observed in the presence of the dual-cation electrolyte cannot be ascribed to a difference in Li⁺ carrier numbers, active sites, or SEI layer. In contrast, the ionic conductivity does change a lot, suggesting that this phenomenon is responsible for the change in pre-exponential factors. Such an increase of the A_0 suggests an increased Li⁺ concentration available at the LTO surface.

To pursue this notion, we note that reversible Li⁺ insertion/deinsertion at the LTO//electrolyte interface is not the sole process related to charge-transfer resistance; also relevant is the ionic conduction in the LTO electrode. As shown in Figure 6, in the thick electrode, distribution of electrolyte potential (φ_{ion}) takes place between the current collector and the electrolyte bulk side, which slows the reaction rate and causes large charge-transfer resistance at the current collector side.²⁹ This potential decrease results in a lower reaction rate and a large charge-transfer resistance (R_{ct}) in the thick electrodes. In case of the single-cation electrolyte, only solvated Li⁺ acts as an ion conductor; thus, its slow ionic conduction caused polarization of the electrolyte potential (φ_{ion}) and decreasing of the electrode potential (E_x); as a result, the local Li⁺ concentration for the Li⁺ intercalation reaction decreases, and the charge-transfer resistance increases. In contrast, in case of dual-cation electrolyte, both solvated Li⁺ and SBP⁺ are ionic conductors; high ionic conduction of the supporting SBP⁺ decreases the polarization and the reaction current increased, which leads to an increase in the available Li⁺ concentration and a lower charge-transfer resistance decrease. The presence of supporting electrolyte enhances Li⁺ transport by suppressing migration limitation, which is responsible for the low power performance of the thick LTO electrodes. Finally, it is worth mentioning that the dual-cation electrolyte system provides better cyclability as shown in Figure S8: 86% capacity retention over 1000 cycles at a current density of 5 mA cm⁻², as compared to that of the single-cation electrolyte (72%). The reasons behind such cyclability improvements are currently under investigation.

4. CONCLUSION

The improved output capabilities observed for cells using dual-cation electrolytes (adding supporting SBPBF₄ electrolyte) with thick electrodes of a few 100 μm are explained by two key parameters. First, the electrolyte ionic conductivity is higher

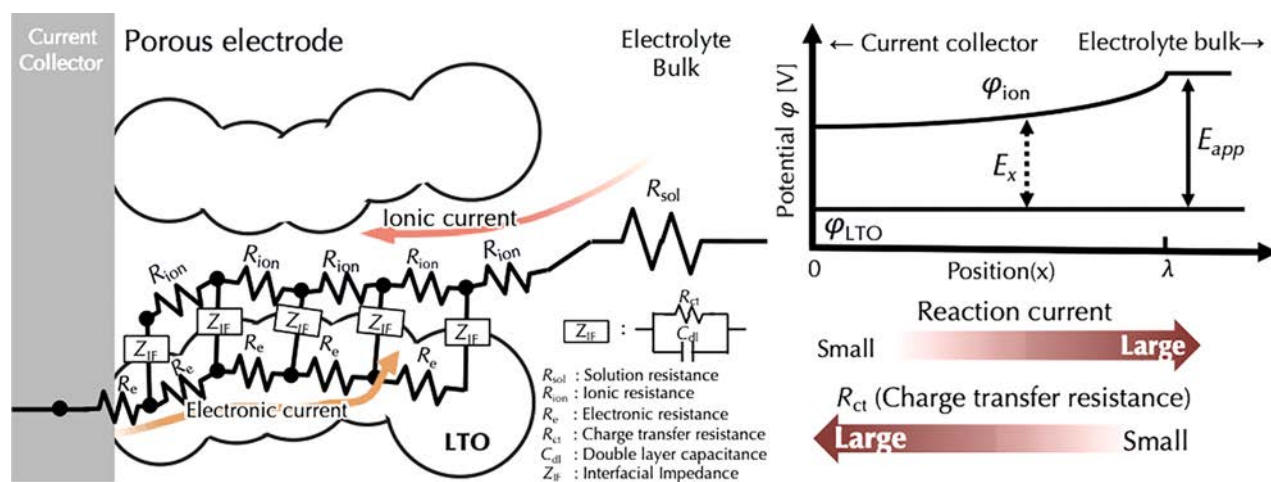


Figure 6. Polarization of the electrolyte potential and charge-transfer resistance in the thick electrodes.²⁹ Here, ϕ_{ion} is the distribution of electrolyte potential, ϕ_{LTO} is the potential of LTO negative electrode, x is the position inside the electrode (current collector side, 0; electrolyte bulk side, λ), E_{app} is the applied voltage at the electrolyte bulk, and E_x is the local voltage in the electrode at a distance (x) from the current collector.

for dual-cation as compared to single-cation electrolytes, decreasing ohmic drops. However, also important is the number of ionic species available during the process of Li^+ insertion into LTO electrodes. In the single-cation electrolyte, only solvated Li^+ is available for ionic conducting, and migration of Li^+ in the electrolyte bulk is assumed to be the rate-limiting factor, resulting in important polarization. In contrast, in the dual-cation case, both solvated Li^+ and SBP^+ act as ionic conductors in the thick LTO electrode, while at the same time migration is rarely rate-limiting and transport-related polarizations are reduced. The key point is that the presence of SBP^+ , despite slowing Li^+ transport through the bulk electrolyte, increases the overall ionic conductivity of the electrolyte, reducing both electrolyte and charge-transfer resistance at the LTO electrode. Thus, this kinetics enhancement makes the addition of a supporting electrolyte an extremely attractive option for increasing the output power density of thick electrode hybrid capacitors.

■ ASSOCIATED CONTENT

SI Supporting Information

The Supporting Information is available free of charge at <https://pubs.acs.org/doi/10.1021/acs.jpcc.0c01916>.

Complementary figures, pertaining to the cell configuration of the four electrode cells (Figure S1), detailed discharge characteristics (Figures S2 and S3), cyclic voltammetric analysis (Figure S4), and spectroscopic analyses: Raman (Figure S5), NMR (Figure S6), EIS (Figure S7), and then cyclability (Figure S8) (PDF)

■ AUTHOR INFORMATION

Corresponding Authors

Etsuro Iwama – Department of Applied Chemistry and Global Innovation Research Organization, Tokyo University of Agriculture & Technology, Koganei, Tokyo 184-8558, Japan; orcid.org/0000-0001-6496-4050; Email: iwama@cc.tuat.ac.jp

Katsuhiko Naoi – Department of Applied Chemistry, Global Innovation Research Organization, and Advanced Capacitor Research Center, Tokyo University of Agriculture & Technology,

Koganei, Tokyo 184-8558, Japan; orcid.org/0000-0002-0265-2235; Email: k-naoi@cc.tuat.ac.jp

Authors

Yu Chikaoka – Department of Applied Chemistry, Tokyo University of Agriculture & Technology, Koganei, Tokyo 184-8558, Japan

Tsukasa Ueda – Department of Applied Chemistry, Tokyo University of Agriculture & Technology, Koganei, Tokyo 184-8558, Japan

Natsuki Miyashita – Department of Applied Chemistry, Tokyo University of Agriculture & Technology, Koganei, Tokyo 184-8558, Japan

Shinichi Seto – Department of Applied Chemistry, Tokyo University of Agriculture & Technology, Koganei, Tokyo 184-8558, Japan

Masato Sakurai – Department of Applied Chemistry, Tokyo University of Agriculture & Technology, Koganei, Tokyo 184-8558, Japan

Wako Naoi – Division of Art and Innovative Technologies, K & W Inc., Kunitachi, Tokyo 186-0002, Japan

McMahon Thomas Homer Reid – Global Innovation Research Organization, Tokyo University of Agriculture & Technology, Koganei, Tokyo 184-8558, Japan; Simpetus LLC, Somerville, Massachusetts 02143, United States

Patrice Simon – Global Innovation Research Organization, Tokyo University of Agriculture & Technology, Koganei, Tokyo 184-8558, Japan; CIRIMAT, Université de Toulouse, CNRS, INPT, UPS, Toulouse 31062 Cedex 9, France; Réseau sur le Stockage Electrochimique de l'Energie, RS2E FR CNRS 3459, Amiens 80039, France; orcid.org/0000-0002-0461-8268

Complete contact information is available at:

<https://pubs.acs.org/doi/10.1021/acs.jpcc.0c01916>

Notes

The authors declare no competing financial interest.

■ ACKNOWLEDGMENTS

This study was supported by the Global Innovation Research Organization in TUAT. This study was supported by JSPS Grant-in-Aid for Scientific Research (KAKENHI) C under grant no. JP17K05962, KAKENHI Grant-in-Aid for Young

Scientists B under grant no. JP16K17970, and the Adaptable and Seamless Technology transfer program through target-driven R&D from the Japan Science and Technology Agency (A-STEP; AS282S002d).

REFERENCES

- (1) Long, J. W.; Bélanger, D.; Brousse, T.; Sugimoto, W.; Sassin, M. B.; Crosnier, O. Asymmetric Electrochemical Capacitors—Stretching the Limits of Aqueous Electrolytes. *MRS Bull.* **2011**, *36*, 513–522.
- (2) Simon, P.; Gogotsi, Y. Materials for Electrochemical Capacitors. *Nanoscience and Technology: A Collection of Reviews from Nature Journals*; World Scientific: River Edge, NJ, 2010; pp 320–329.
- (3) Amatucci, G. G.; Badway, F.; Du Pasquier, A.; Zheng, T. An Asymmetric Hybrid Nonaqueous Energy Storage Cell. *J. Electrochem. Soc.* **2001**, *148*, A930–A939.
- (4) Naoi, K.; Ishimoto, S.; Miyamoto, J.-i.; Naoi, W. Second Generation ‘Nanohybrid Supercapacitor’: Evolution of Capacitive Energy Storage Devices. *Energy Environ. Sci.* **2012**, *5*, 9363–9373.
- (5) Augustyn, V.; Simon, P.; Dunn, B. Pseudocapacitive Oxide Materials for High-Rate Electrochemical Energy Storage. *Energy Environ. Sci.* **2014**, *7*, 1597–1614.
- (6) Shao, Y.; El-Kady, M. F.; Sun, J.; Li, Y.; Zhang, Q.; Zhu, M.; Wang, H.; Dunn, B.; Kaner, R. B. Design and Mechanisms of Asymmetric Supercapacitors. *Chem. Rev.* **2018**, *118*, 9233–9280.
- (7) Shi, X.; Zhang, W.; Wang, J.; Zheng, W.; Huang, K.; Zhang, H.; Feng, S.; Chen, H. (EMIm)⁺(PF₆)⁻ Ionic Liquid Unlocks Optimum Energy/Power Density for Architecture of Nanocarbon-Based Dual-Ion Battery. *Advanced Energy Materials* **2016**, *6*, 1601378.
- (8) Shi, X.; Yu, S.; Deng, T.; Zhang, W.; Zheng, W. Unlock the Potential of Li₄Ti₅O₁₂ for High-Voltage/Long-Cycling-Life and High-Safety Batteries: Dual-Ion Architecture Superior to Lithium-Ion Storage. *J. Energy Chem.* **2020**, *44*, 13–18.
- (9) Zheng, H.; Li, J.; Song, X.; Liu, G.; Battaglia, V. S. A Comprehensive Understanding of Electrode Thickness Effects on the Electrochemical Performances of Li-Ion Battery Cathodes. *Electrochim. Acta* **2012**, *71*, 258–265.
- (10) Ogihara, N.; Itou, Y.; Sasaki, T.; Takeuchi, Y. Impedance Spectroscopy Characterization of Porous Electrodes under Different Electrode Thickness Using a Symmetric Cell for High-Performance Lithium-Ion Batteries. *J. Phys. Chem. C* **2015**, *119*, 4612–4619.
- (11) Naoi, K. ‘Nanohybrid Capacitor’: The Next Generation Electrochemical Capacitors. *Fuel Cells* **2010**, *10*, 825–833.
- (12) Xu, K. Nonaqueous Liquid Electrolytes for Lithium-Based Rechargeable Batteries. *Chem. Rev.* **2004**, *104*, 4303–4418.
- (13) Yamada, Y.; Furukawa, K.; Sodeyama, K.; Kikuchi, K.; Yaegashi, M.; Tateyama, Y.; Yamada, A. Unusual Stability of Acetonitrile-Based Superconcentrated Electrolytes for Fast-Charging Lithium-Ion Batteries. *J. Am. Chem. Soc.* **2014**, *136*, 5039–5046.
- (14) Dokko, K.; Watanabe, D.; Ugata, Y.; Thomas, M. L.; Tsuzuki, S.; Shinoda, W.; Hashimoto, K.; Ueno, K.; Umebayashi, Y.; Watanabe, M. Direct Evidence for Li Ion Hopping Conduction in Highly Concentrated Sulfolane-Based Liquid Electrolytes. *J. Phys. Chem. B* **2018**, *122*, 10736–10745.
- (15) Yamada, Y.; Wang, J.; Ko, S.; Watanabe, E.; Yamada, A. Advances and Issues in Developing Salt-Concentrated Battery Electrolytes. *Nature Energy* **2019**, *4*, 269–280.
- (16) Hayamizu, K.; Aihara, Y.; Nakagawa, H.; Nukuda, T.; Price, W. S. Ionic Conduction and Ion Diffusion in Binary Room-Temperature Ionic Liquids Composed of [Emim][BF₄] and LiBF₄. *J. Phys. Chem. B* **2004**, *108*, 19527–19532.
- (17) Iwama, E.; Ueda, T.; Ishihara, Y.; Ohshima, K.; Naoi, W.; Reid, M. T. H.; Naoi, K. High-Voltage Operation of Li₄Ti₅O₁₂/Ac Hybrid Supercapacitor Cell in Carbonate and Sulfone Electrolytes: Gas Generation and Its Characterization. *Electrochim. Acta* **2019**, *301*, 312–318.
- (18) Azais, P.; Tamic, L.; Huitric, A.; Paulais, F.; Rohel, X. Separator Film, Its Fabrication Method, Supercapacitor, Battery and Capacitor Provided with Said Film. US. Patent US9,461,288, Oct. 4, 2016.
- (19) Come, J.; Taberna, P.-L.; Hamelet, S.; Masquelier, C.; Simon, P. Electrochemical Kinetic Study of LiFePO₄ Using Cavity Microelectrode. *J. Electrochem. Soc.* **2011**, *158*, A1090–A1093.
- (20) Conway, B. E. *Electrochemical Supercapacitors: Scientific Fundamentals and Technological Applications*; Kluwer Academic/Plenum Press: New York, 1999.
- (21) Ishihara, Y.; Miyazaki, K.; Fukutsuka, T.; Abe, T. Kinetics of Lithium-Ion Transfer at the Interface between Li₄Ti₅O₁₂ Thin Films and Organic Electrolytes. *ECS Electrochem. Lett.* **2014**, *3*, A83–A86.
- (22) Ogumi, Z. Interfacial Reactions of Lithium-Ion Batteries. *Electrochemistry* **2010**, *78*, 319–324.
- (23) Doi, T.; Iriyama, Y.; Abe, T.; Ogumi, Z. Pulse Voltammetric and Ac Impedance Spectroscopic Studies on Lithium Ion Transfer at an Electrolyte/Li₄/3Ti₅/3O₄ Electrode Interface. *Anal. Chem.* **2005**, *77*, 1696–1700.
- (24) Xu, K.; von Cresce, A.; Lee, U. Differentiating Contributions to “Ion Transfer” Barrier from Interphasial Resistance and Li⁺ Desolvation at Electrolyte/Graphite Interface. *Langmuir* **2010**, *26*, 11538–11543.
- (25) Nakayama, N.; Nozawa, T.; Iriyama, Y.; Abe, T.; Ogumi, Z.; Kikuchi, K. Interfacial Lithium-Ion Transfer at the LiMn₂O₄ Thin Film Electrode/Aqueous Solution Interface. *J. Power Sources* **2007**, *174*, 695–700.
- (26) Takeuchi, M.; Kameda, Y.; Umebayashi, Y.; Ogawa, S.; Sonoda, T.; Ishiguro, S.-i.; Fujita, M.; Sano, M. Ion–Ion Interactions of LiPF₆ and LiBF₄ in Propylene Carbonate Solutions. *J. Mol. Liq.* **2009**, *148*, 99–108.
- (27) Yamada, I.; Iriyama, Y.; Abe, T.; Ogumi, Z. Lithium-Ion Transfer on a Li_xCoO₂ Thin Film Electrode Prepared by Pulsed Laser Deposition—Effect of Orientation. *J. Power Sources* **2007**, *172*, 933–937.
- (28) Joshi, P.; Iwai, K.; Patnaik, S. G.; Vedarajan, R.; Matsumi, N. Reduction of Charge-Transfer Resistance Via Artificial Sei Formation Using Electropolymerization of Borylated Thiophene Monomer on Graphite Anodes. *J. Electrochem. Soc.* **2018**, *165*, A493–A500.
- (29) Zyun, S.; Susumu, K.; Hajime, M. *Electrochemical Impedance*; Tokyo Kagaku Dojin: Kyoto, Japan, 2019.